Using experimental design to assess rate-dependent numerical models

Citation for the original published paper (version of record):
Tahershamsi, H., Dijkstra, J. (2022). Using experimental design to assess rate-dependent numerical models. Soils and Foundations, 62(6). http://dx.doi.org/10.1016/j.sandf.2022.101244

HOSTED BY

ELSEVIER

Available online at www.sciencedirect.com

ScienceDirect

Soils and Foundations 62 (2022) 101244

SOILS AND FOUNDATIONS

www.elsevier.com/locate/sandf

Technical Paper

Using experimental design to assess rate-dependent numerical models

Hossein Tahershamsi *, Jelke Dijkstra

Chalmers University of Technology, Department of Architecture and Civil Engineering, SE-41296 Gothenburg, Sweden

Received 25 April 2022; received in revised form 14 October 2022; accepted 1 November 2022

Abstract

To enhance the accuracy of advanced constitutive models for soft natural clays, several parameters are necessary, resulting in complexity of numerical modelling. However, the detailed effects of these parameters are not rigorously quantified towards their constitutive relationships. Thus, the aim of the paper is to assess such advanced models in order to determine the most significant parameters over the time series data. Two methods for Global Sensitivity Analysis (GSA), *i.e.* Experimental Design and the Sobol method, were used and benchmarked to assess the model predictions on a discretised domain in time and space. A rate-dependent Finite Element model using Creep-SCLAY1S and a hydro-mechanically coupled formulation for consolidation was used to study a Constant Rate of Strain (CRS) test. The value of GSA approaches adopted herein was to investigate the model predictions both in the temporal and spatial domain. The temporal analyses indicate three sets of significant model parameters in different portions of the CRS compression curve. Furthermore, the non-stationary nature of sensitivity results is exposed, identifying the parameters that lead to unique solutions for the CRS loading path. The FE implementation enabled the quantification of the most sensitive model parameters in the spatial domain. The spatial results that are governed by the rate-dependent processes in the soil (*i.e.* consolidation and creep) illustrated that Experimental Design was capable of providing sensitivity maps with satisfactory accuracy similar to the Sobol method. Experimental Design was found to be the most efficient method, concerning execution time and storage costs, to assess rate-dependent problems in Geotechnics.

Keywords: Experimental design; Rate-dependent models; Constant Rate of Strain (CRS); Global Sensitivity Analysis (GSA); Sobol method; Model assessment

1. Introduction

The evolving mechanical response of saturated fine-grained soils is governed by two time-dependent processes: consolidation that relates to flow of water, and substantial creep rates exhibited by intact natural clays. Modelling these phenomena requires coupled hydro-mechanical analyses including rate-dependent constitutive models by adopting the Finite Element (FE) method (Rowe and Hinchberger, 1998; Potts and Zdravkovic, 2001).

Such models contain a large number of features, with associated parameters, to capture the soil behaviour with sufficient accuracy (Muir Wood, 2004). Natural clays that have been subjected to geological, geo-environmental and anthropogenic processes are weakly bonded, showing an anisotropic and rate-dependent response (Leroueil and Vaughan, 1990; Mitchell and Soga, 2005). Thus, more complex constitutive models have been developing over the last two decades (Wheeler et al., 2003; Karstunen et al., 2005; Masin, 2005; Dafalias et al., 2006; Yin et al., 2010; Sivasithamparam et al., 2015; Gras et al., 2018). The features implemented, however, require a systematic calibration effort to derive the model parameters, which for complex models with limited data may become non-unique (*e.g.* Gras et al., 2017; Yin et al., 2018). In order

Peer review under responsibility of The Japanese Geotechnical Society.
* Corresponding author.
E-mail addresses: hossein.tahershamsi@chalmers.se (H. Tahershamsi), jelke.dijkstra@chalmers.se (J. Dijkstra).

https://doi.org/10.1016/j.sandf.2022.101244
0038-0806/

Nomenclature

SA	Sensitivity Analysis
GSA	Global Sensitivity Analysis
CRS	Constant Rate of Strain
OFAT	One-Factor-At-a-Time
RFEM	Random Finite Element Method
FE	Finite Element
1D	one-dimensional
2D	two-dimensional
MOE	Margin of Error
OCR	Over-consolidation ratio
DOE	Design of Experiments
NCS	Normal Consolidation Surface
CSS	Current Stress Surface
ICS	Intrinsic Compression Surface
S_i	Sobol's first-order index
S_T	Sobol's total-order index
$\mathbf{C}$	contrast matrix
$\mathbf{R}$	response vector
$\mathbf{E}$	vector of effects
K	hydraulic conductivity
k	number of input factors
N	Monte Carlo sample size
κ^*	modified swelling index
ν'	Poisson's ratio
λ_i^*	modified intrinsic compression index
M_c	slope of critical state line in triaxial compression
M_e	slope of the critical state line in triaxial extension
σ'_{p_0}	initial pre-consolidation pressure
α_0	initial inclination of NCS
ω	absolute effectiveness of rotational hardening
ω_d	relative effectiveness of rotational hardening
χ_0	initial amount of bonding
a	absolute rate of destructuration
b	relative rate of destructuration
μ_i^*	intrinsic modified creep index
τ	reference time
u	consolidation
F_{err}	misfit function
$\epsilon^e_{v,d}$	elastic volumetric and deviatoric strain rate, respectively
$\epsilon^c_{v,d}$	viscoplastic volumetric and deviatoric strain rate, respectively
p'	mean effective stress
p'_{eq}	equivalent mean effective stress
p'_m	mean effective preconsolidation pressure
q	deviatoric stress
Λ	rate-dependent viscoplastic multiplier

to avoid commonplaces during calibration processes, the aim of the study is to introduce Experimental Design as an initial step to assess geotechnical rate-dependent problems using Finite Element (FE) analysis.

In Geotechnics, the amount of available experimental data with which to develop and calibrate constitutive models is limited, especially when considering the large dimension of a typical field investigation. Thus, in a statistical sense, the ratio of the number of samples to the population size is extremely small (Journel and Alabert, 1989). Hence, the extent of the site investigation, *e.g.* the number of *in situ* or laboratory tests, type of tests and test location, directly influence the costs of foundation systems (Crisp et al., 2021). As a result, statistical approaches are required to deal with the sources of uncertainty in subsurface exploration. Besides, numerical models are always idealisations of real problems; therefore, the predicted geomechanical response involves uncertainty (Phoon and Kulhawy, 1999).

To include the impacts of uncertainty which originates from defects in subsurface exploration, and ultimately numerical models, several strategies have been followed using the Random Finite Element Method (Griffiths and Fenton, 1993; Fenton and Griffiths, 1993). RFEM follows an advanced probabilistic technique by elegantly incorporating spatial heterogeneity with random fields (Fenton and Vanmarcke, 1990). So far, in most applications of RFEM, the focus has been on demonstrating the method for certain engineering applications, using somewhat simplified and idealised constitutive models. More advanced constitutive models are required to capture the *in situ* soil response. Some of the data assimilation methods show more accurate predictions using more complex constitutive models that incorporate extra features, such as anisotropy, non-linearity and spatial variability (*e.g.* Nishimura et al., 2002; Nishimura et al., 2005). To study such advanced models rigorously, a systematic method for Sensitivity Analysis (SA) that overcomes the limitations of One-Factor-At-a-Time (OFAT) method is required (Czitrom, 1999). When more practical techniques are required, Global Sensitivity Analysis (GSA) methods offer the best trade-off between efficiency and non-linearity of models. The term *Global Sensitivity Analysis* refers to specific SA techniques that explore the entire range of input factors within a plausible domain. Examples of GSA methods include the variance-based method of Sobol, the Elementary Effects method, and Experimental Design (Saltelli and Annoni, 2010).

In recent years, the usage of GSA methods for model evaluation has been increasing. Although GSA methods have been extensively used in many scientific disciplines, they are less used in engineering practice (Ferretti et al., 2016). To simulate underground construction activities, GSA methods were early on adapted to soil-structure effects from mechanised tunnelling (Miro et al., 2014; Liu

et al., 2017; Zhao et al., 2018) and thermally activated pile foundations (Shao et al., 2021), most often for simple constitutive models. Gras et al. (2017) conducted the Sobol method as part of identifying the model parameters from artificial data by formulating an inverse analysis as an optimisation problem. For the state-of-the-art on inverse analysis and methods to estimate model parameters see Tarantola (2005). To date, the Sobol method has most frequently been used (*e.g.* Khaledi et al., 2016; Zhao et al., 2018; Mahmoudi et al., 2019; Fang and Su, 2020; Shao et al., 2021), whereas another possibility and yet relatively unexplored approach is Experimental Design (Box et al., 2009).

In this paper, a diagnostic method, based on statistical Experimental Design, is developed for temporal and spatial analyses of boundary value problems in Geotechnics. A fractional factorial design, together with a temporal misfit function, is used to assess the parameters related to a rate-dependent constitutive model, Creep-SCLAY1S (Karstunen et al., 2005; Sivasithamparam et al., 2015; Gras et al., 2018). Creep-SCLAY1S includes many features of soft natural clays and has been successfully validated against full scale field problems, including common geotechnical problems, such as embankment loading and deep excavation in soft clays (Amavasai et al., 2018; Tornborg et al., 2021). The assessment probes the true ranges of model parameters, *i.e.* obtained from calibration of FE model with experimental data from laboratory. The paper illustrates that such an assessment is essential for advanced constitutive models prior to use in calibration processes, data assimilation, and RFEM. The methods presented herein are generic, therefore suitable for further assessment of any constitutive or system-level problems in Civil Engineering.

2. Methods of global sensitivity analysis

Performing Sensitivity Analysis (SA) often involves One-Factor-At-a-Time (OFAT) plans to examine their impact on the desired model response. Such an approach is not optimal in terms of quantifying the relative importance of model parameters and their interactions in a particular assessment. The major purpose of conducting a GSA is to find the ranking of the most uncertain factors. Another intention is to simplify the models by fixing non-influential factors within their respective domains (Saltelli et al., 2008). The latter is especially advantageous for hierarchical constitutive models developed in Geotechnics, as not all model features, with their associated model parameters, are required for a given stress path. The GSA techniques used in this study are discussed briefly in the following.

2.1. Sobol method

The Sobol method is a variance-based approach that takes into account the variance of the output. The method, based on Sobol' (1993), was further developed for sensitivity analysis of nonlinear mathematical models by using a Monte Carlo sampling scheme (Saltelli, 2002). The Sobol method offers great advantages because of its model independency and the capability of quantifying the interaction effects. Moreover, the method probes the obscurely multi-dimensional space of input factors by using a prescribed number of random Monte Carlo maps (Saltelli et al., 2008). When investigating k number of factors, by considering a deterministic analytical function f, the total variance of the function $V(f)$ is:

$$V(Y) = \sum_{i=1}^{k} V_i + \sum_{i}\sum_{i<j} V_{ij} + \ldots + V_{12\ldots k} \tag{1}$$

In Eq. (1), V_i is the first-order variance from i^{th} parameter, V_{ij} represents the second-order contribution from the interaction between factors i and j. The remaining higher-order interactions are considered up to $V_{1,\ldots,p}$, *i.e.* the interactions between all factors. By normalising the first-order variance over the total variance of the model, the first-order index S_i is calculated; see Eq. (2):

$$S_i = \frac{V_i}{V} \tag{2}$$

The first-order index indicates the main contribution of each factor to the variance of the chosen response. S_i only quantifies the order of influence for each factor, and is thus useful for factor prioritisation purposes. When investigating nonlinear models, the contribution of the higher-order variances should also be involved. This becomes evident by dividing Eq. (4) by total variance $V(f)$ on both sides of the equation; see Eq. (3).

$$\sum_{i=1}^{k} S_i + \sum_{i}\sum_{1\leqslant i<j\leqslant p} S_{ij} + \sum_{i}\sum_{i<j}\sum_{i<j<m} S_{ijm} + \ldots + S_{12\ldots k} = 1 \tag{3}$$

An efficient approach was proposed by Homma and Saltelli (1996) to measure the total-order index at the same cost as the first-order indices. The total-order effect is obtained by normalising the first-order variance, excluding i^{th} factor (*i.e.* $V_{\sim i}$), with a total variance of the model V and later subtracting from one; see Eq. (4).

$$S_{T_i} = 1 - \frac{V_{\sim i}}{V} \tag{4}$$

The total-order index S_{T_i} quantifies the possible interactions of model parameters, if there is a significant difference between the first-order and the total-order index of particular model parameter. The total-order index is commonly used to screen parameters of least importance.

2.2. Experimental design and factorial design

The *Experiment* refers to the operation of a system with k input factors adjusted for some definite set of levels. When investigating a process or system, such as a

geotechnical FE model, the special arrangement of points chosen to study a model response relationship is called an *Experimental Design* (Box and Draper, 1987). Thus, the reader should be careful not to associate *Experimental Design* with geotechnical tests that are carried out either in a laboratory or in the field. *Factorial design*, based on Experimental Design, is a statistical method varying all factors simultaneously. In this method, a fixed number of levels are assigned to each factor studied in the model. The impacts of all possible combinations of factor levels are quantified for a selected model response (Box et al., 2009). The average response from combinations of factors is denoted as the *main effect*. This implies that the results are valid only within the parameter space studied with factorial design. As an example, a 2^2 full design is conducted in Table 1. Here, two different levels respectively corresponding to the lower and upper bound of each model parameter, are assigned to factors A and B.

Subsequently, a *table of contrast* that includes the total number of possible combinations of levels is constructed; see Table 2. The table contains the total number of realisations, followed by two columns of *main effects*, A, B, and column AB representing the interaction of parameters. Each model response is shown as a single observation y in the last column of Table 2.

The main and interaction effects of the factors are calculated as follows:

$$\mathbf{E} = \frac{2}{n_{\text{runs}}} \underbrace{\begin{bmatrix} -1 & -1 & +1 \\ +1 & -1 & -1 \\ -1 & +1 & -1 \\ +1 & +1 & +1 \end{bmatrix}^{\mathsf{T}}}_{\mathbf{C}} \underbrace{\begin{bmatrix} y_1 \\ y_2 \\ y_3 \\ y_4 \end{bmatrix}}_{\mathbf{R}} = \begin{bmatrix} A_{\text{main.}} \\ B_{\text{main.}} \\ AB_{\text{int.}} \end{bmatrix} \tag{5}$$

In Eq. (5), **C** is the contrast matrix, **R** the response vector, **E** the vector of effects and n_{runs} denotes the total number of runs in a two-level factorial design. $A_{\text{main.}}$ and $B_{\text{main.}}$ are the calculated main effects, whereas $AB_{\text{int.}}$ is the measured *interaction effect* between factors A and B.

It is possible to reduce the number of simulations by using only a fraction of the full factorial design at the expense of neglecting the high-order interaction effects. Thus, fractional factorial designs will reduce the number of simulations by confounding some interaction effects with main effects. In such designs, the *Resolution* governs the degree of confounding. A design with Resolution IV does not confound main effects with other main effects or two-factor interactions. However, two-factor interactions are aliased with each other (Montgomery, 2009). In this study, the fractional factorial is used for screening purposes.

Table 1
Levels of factors: a 2^2 example.

	Levels	
Factors	−	+
A	A^-	A^+
B	B^-	B^+

Table 2
Table of contrast with coefficients for the 2^2 full factorial design.

Run #	A	B	AB	Response, y
1	−	−	+	y_1
2	+	−	−	y_2
3	−	+	−	y_3
4	+	+	+	y_4

3. The Finite Element (FE) model

The Constant Rate of Strain (CRS) test is a common geotechnical tests that includes rate-dependency and hydro-mechanical response. Since the mobilisation of excess porewater pressures at large levels of strain is non-uniform, a system-level interpretation is essential for the numerical modelling of a CRS test (Muir Wood, 2016). Thus, rather than evaluating the behaviour of a constitutive model in isolation at a single integration point, discretisation of the boundary value problem is required. Solving some differential equations (*e.g.* the balance principle and groundwater flow) where specific information is known a *priori* for the unknowns at the boundary is denoted as the boundary value problem (Ottosen and Petersson, 1992). The constitutive model used for boundary value problem of CRS test is Creep-SCLAY1S, for which a brief overview has been provided in Section A. Creep-SCLAY1S model was developed based on Modified Cam Clay (Roscoe and Burland, 1968), and was gradually expanded further to model the behaviour of natural soft clays, which often are sensitive. Thus, additional model features were introduced gradually to include anisotropy, the presence of bonds in sensitive clays and the degradation of bonds, as well as rate-dependency (Karstunen et al., 2005; Sivasithamparam et al., 2015; Gras et al., 2018).

In this study, a Finite Element (FE) model with 2D axisymmetric geometry of a CRS test, with the dimensions of 50 mm diameter and 20 mm height, was created in Tochnog Professional FE software[1]. Fig. 1 shows the FE mesh and boundary conditions of the numerical model. The types of elements were 6-noded triangles with second-order shape functions. The mesh was fixed in both directions at the bottom boundary and horizontally fixed on the sides, thus representing oedometric conditions. The water in the sample drains from the top boundary and cannot drain from remaining boundaries.

An initial isotropic compressive stress of 5 kPa was prescribed within the sample. Throughout this study, geotechnical sign convention is used, with compression positive. Similar to the laboratory tests, the samples were axially loaded by prescribing a constant rate of displacement on

[1] A user supplied material subroutine of Creep-SCLAY1S was applied.

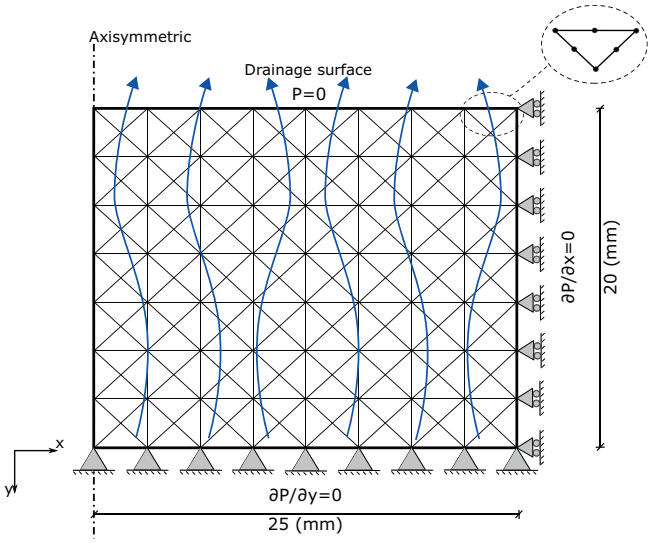

Fig. 1. FE mesh, geometry, and boundary conditions. P denotes the porewater pressure.

the top boundary, until an ultimate axial strain of 30 % was reached.

The present study was performed with a displacement rate of 0.0024 mm min^{-1} for temporal SA, following the standard Swedish practice. Additionally, the effect of displacement rate was investigated with spatial SA. The groundwater flow and consolidation were solved using the storage equation that is coupled to the material deformations via the volumetric strain (Verruijt, 2015).

The hydraulic conductivity K was set to a value comparable to what is found in Swedish sensitive clays, *i.e.* 8×10^{-5} m d^{-1} (Karlsson et al., 2016). The effect of soil stratification on hydraulic conductivity was considered by selecting the ratio $K_{max}/K_{min} \approx 3$ (Kashef, 1986).

3.1. The misfit function

A misfit function with a least-squares criterion is introduced to capture the sensitivity of factors. The typical compression curve from CRS testing is used for quantifying the misfit function. Hence, the shape of the compression curve over a continuous time series has been examined to study the temporal sensitivity of the factors (Tarantola, 2005; Papon et al., 2012). The misfit function measures the difference between the *reference* response with respect to the *realisations*, *i.e.* generated from GSA methods. Subsequently, the least-square term was normalised with the area under the reference curve at final time series A^n_{ref}. Thus, the misfit function becomes a dimensionless scalar; see Eq. (6).

$$F_{err}(\boldsymbol{X})|_0^{t_n} = \sqrt{\sum_{i=1}^{n}\left|\frac{A^i_{ref} - A^i_{real}(\boldsymbol{X})}{A^n_{ref}}\right|^2} \tag{6}$$

In Eq. (6), $\boldsymbol{X}|_0^{t_n}$ is the vector of the factors over the temporal domain, $A^i_{ref} = \sum_{i=1}^{n}\varepsilon_{ref}\Delta\sigma'_i$ is the area under the curve resulting from reference input factors. In this study, the calibrated numerical model in Section 4 is considered to be the reference case. $A^i_{real} = \sum_{i=1}^{n}\varepsilon_{real}\Delta\sigma'_i$ presents the area under the curve from realisations, *i.e.* originated from GSA methods. All areas are measured using the trapezoidal rule, in which n represents the total number of intervals for integrating the areas below the curve. The schematic interpretation of the misfit function is displayed in Fig. 2.

The temporal analysis of the misfit function illustrates the most significant factors at different instances of consolidation. It has been demonstrated that the response of overconsolidated soil specimens during confined compression are different from normally consolidated samples due to their disparate hydro-mechanical behaviour (Peck et al., 1974). Thus, for performing temporal SA, the effective stress–strain behaviour of the soil specimen are separated into three zones shown in Fig. 3.

3.2. Validation of Sobol method

The Sobol method requires a convergence study in order to find the adequate sample size due to the Monte Carlo sampling strategy. In the current study, a crude Monte Carlo sampling technique is utilised leading to the generation of $(2k + 2)N$ model evaluations, where k is the number of model parameters and N is the sample size. For an initial guess, Saltelli et al. (2008) have recommended an N value of between 500 and 1000. The Monte Carlo sampling and subsequent Sobol analyses are calculated using the SALib Python library (Herman and Usher, 2017). The convergence study of FE simulations is presented in Fig. 4, in which the y-axis is the total-order Margin of Error (MOE) within a 95 % confidence interval divided by S_T. Fig. 4 demonstrates that the level of uncertainty is

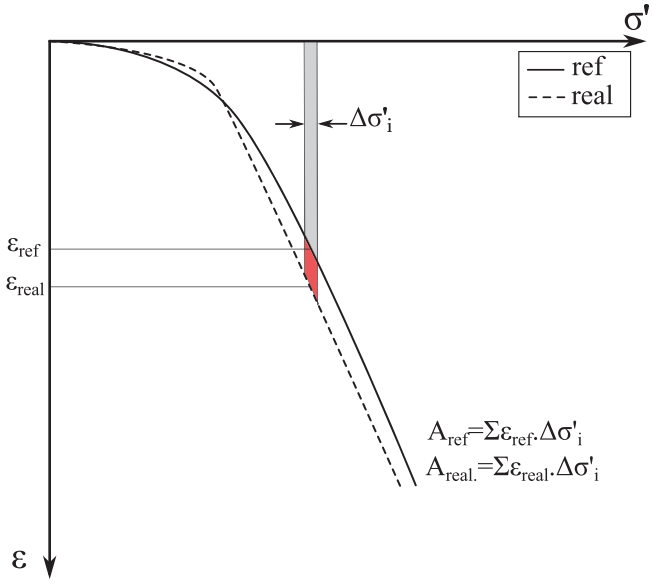

Fig. 2. Definition of the misfit function, where σ' denotes vertical effective stress and ε denotes axial strain.

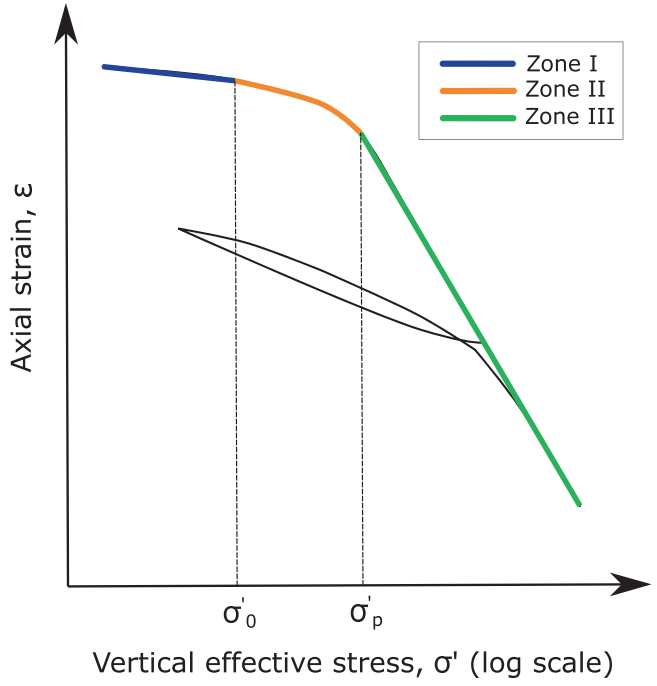

Fig. 3. Definition of zones in effective stress–strain consolidation curve of an overconsolidated sample (Adapted from Peck et al., 1974).

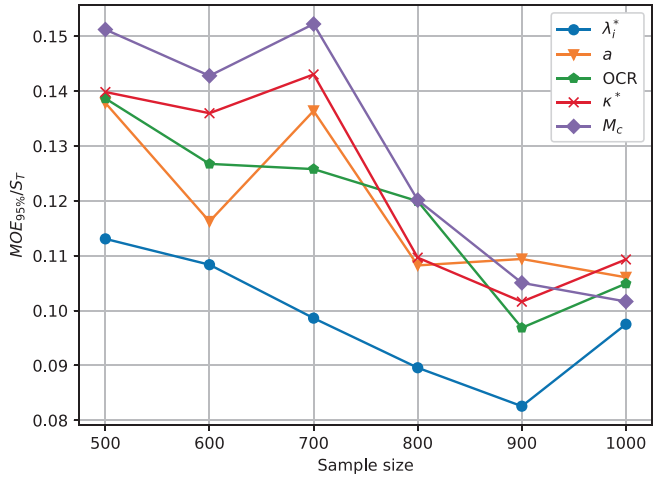

Fig. 4. The convergence study of sample size N for Sobol method.

decreased for all the factors, by increasing the number of samples N. Thus, based on the convergence study performed, 1000 number of samples N is selected for following Sobol analyses in Section 5.2.

In addition, the results of the Sobol method are verified by comparing single element simulations with the corresponding FE model of the CRS test. For this purpose, the identical ranges from Gras et al. (2017) are studied, about which the sensitivity analyses have been performed at single element level. Table 3 presents the ranges of the Creep-SCLAY1S model parameters pertaining to verification of the Sobol method at the FE boundary problem and single element level.

Table 3
Ranges for validation of Sobol results.

		Range I (Gras et al., 2017)		
Factor	Unit	–	+	Relative range(%)
κ^*		0.0225	0.0275	20
ν'		0.18	0.22	20
λ_i^*		0.077	0.094	20
M_c		1.17	1.43	20
M_e		0.81	0.99	20
OCR		1.247	1.525	20
α_0		0.378	0.462	20
ω		29.7	36.3	20
ω_d		0.785	0.959	20
χ_0		18	22	20
a		9	11	20
b		0.36	0.44	20
μ_i^*		1.35×10^{-3}	1.65×10^{-3}	20

Similar to single element simulations and to enable comparison, the FE model for CRS test here does not incorporate a coupled stress-flow procedure. The misfit function at the end of the test represents the response for Sobol verification, where the reference case is defined as the middle range of Table 3 (Gras et al., 2017). The Sobol index S_T obtained from the single element simulations and FE models are presented in Fig. 5. Some differences are observed due to a slightly different definition of compression index. In Gras et al. (2017), instead of the modified intrinsic compression index $\lambda_i^*, \zeta_i^* = \lambda_i^* - \kappa^*$ is used. Furthermore, preconsolidation pressure σ'_{p_0} is used as an input parameter instead, whereas the overconsolidation ratio (OCR) is used in this stage. These differences have no consequence for the comparison, as the non-influential parameters with $S_T \cong 0$ remain the same; see Fig. 5. Thus, the results illustrate the

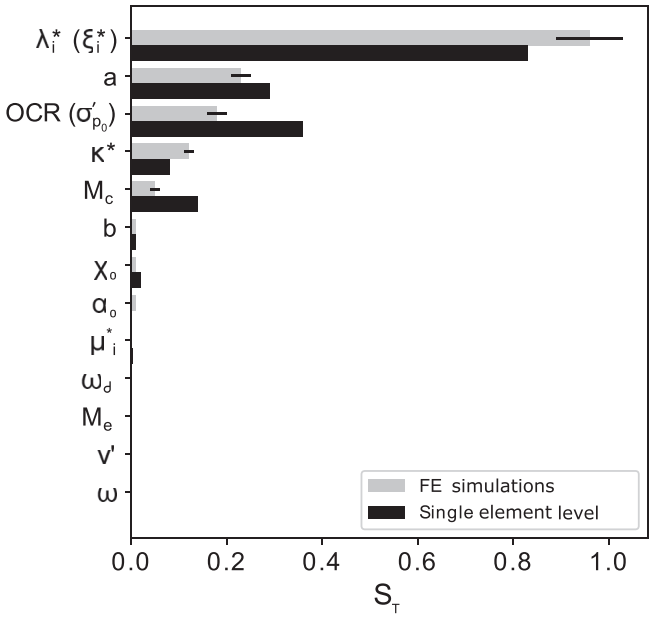

Fig. 5. Comparison of Sobol's S_T between single element level simulations and current FE models.

successful implementation of the Sobol method using FE discretisation, in which no substantial differences have been observed in terms of important factors.

4. Design of Experiments (DOE)

The main significance of our statistical Experimental Design is to investigate true ranges of parameters, as opposed to previous researches (*e.g.* Gras et al., 2017; Yin et al., 2018), which used only artificially generated data. For this purpose, the parameters of the Creep-SCLAY1S model have been calibrated with laboratory data on clay from the Utby test site, *i.e.* located in Gothenburg, Sweden (Karlsson et al., 2016). The model parameters, such as κ^*, λ_i^*, and σ'_{p_0}, were derived manually from the laboratory CRS data. The values for κ^* and λ_i^* respectively represent the elastic and intrinsic slope of the $\ln \sigma'_v - \varepsilon$ curve, where σ'_v denotes the vertical effective stress. The preconsolidation pressure σ'_{p_0} is determined from the CRS laboratory data by using the suggested method in Sallfors (1975). The remaining Creep-SCLAY1S parameters are derived from a set of incremental loading oedometer tests as well as triaxial tests that were sheared in compression and extension (Karstunen and Amavasai, 2017). Table 4 presents the calibrated Creep-SCLAY1S parameters. Fig. 6 displays the good agreement between the FE model and the effective stress–strain behaviour of an undisturbed piston sample from a depth of 8 m.

Based on the calibrated values, a wider range of input parameters is selected, whereby the theoretical and physical limitations of Creep-SCLAY1S parameters in relation to Utby clay are taken into consideration (Karlsson et al., 2016; Gras et al., 2017; Gras et al., 2018). Thus, while it may be that the design is totally universal for any specific set of circumstances, it will deliver feasible response over the range of conditions in which it is likely to be used.

Table 4
Calibration of CRS numerical model with Utby clay.

Factor	Description	Unit	CRS 8 m
κ^*	Modified swelling index	-	0.0124
ν'	Poisson's ratio	-	0.2
λ_i^*	Modified intrinsic compression index	-	0.0894
M_c	Slope of critical state line in triaxial compression	-	1.55
M_e	Slope of the critical state line in triaxial extension	-	1.15
σ'_{p_0}	Initial effective preconsolidation pressure	kPa	90
α_0	Initial inclination of NCS	-	0.63
ω	Absolute effectiveness of rotational hardening	-	30
ω_d	Relative effectiveness of rotational hardening	-	1.014
χ_0	Initial amount of bonding	-	10
a	Absolute rate of destructuration	-	9
b	Relative rate of destructuration	-	0.5
μ_i^*	Intrinsic modified creep index	-	1.42×10^{-3}
τ	reference time	d	1

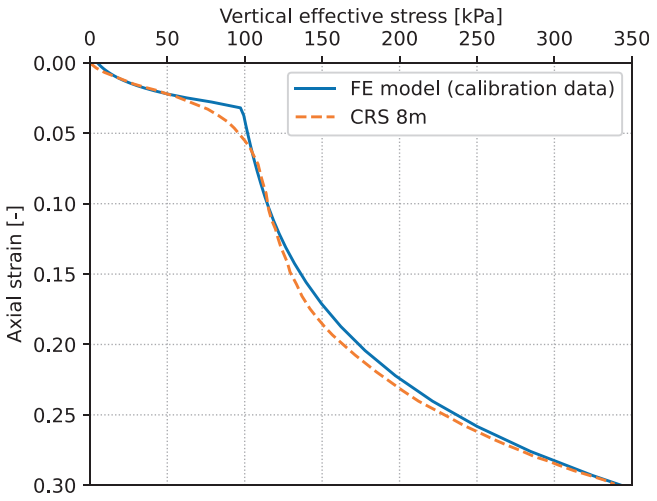

Fig. 6. FE simulation compared to the CRS laboratory data of Karlsson et al. (2016).

The subsequent wider range is denoted as Range II and presented in Table 5. The benefit of DOE is that the main effects obtained for parameters are not just valid for a specific combination of other parameters, providing the values of other parameters remain within their respective ranges that are chosen for the FE simulations.

An extra qualitative factor, *i.e.* consolidation u, is introduced in order to distinguish the influence and mechanism of water flow (consolidation) over the discretised domain. Concerning the 14 factors and their associated levels in Table 5, an Experimental Design was conducted. First, a two-level fractional factorial design was utilised for the purpose of factor screening over the temporal domain of the misfit function. This is quite beneficial since a fraction (*i.e.* one-256th) of the full design requires only $2^{14-9} = 32$ model evaluations. The fractional design is chosen in Resolution IV, meaning that no main effects are confounded with any two-factor interactions. The coded table of contrast for $2^{14-9}_{\mathbf{IV}}$ fractional design is presented in Table 6. The DOE procedure is implemented using pyDOE[2] with which the higher-order interactions are coded by the author.

5. Results and discussion

5.1. Temporal SA of CRS loading path

The sensitivity of Creep-SCLAY1S parameters, over the entire time-series of the CRS loading path, is investigated first. A $2^{14-9}_{\mathbf{IV}}$ factorial design is used with a wider range of factors presented in Table 5. The temporal main effects corresponding to zones defined in Section 3.1 are presented in Figs. 7–9, where the positive effects are illustrated by black colour bars, whereas the negative effects are presented by grey colour bars.

[2] https://pythonhosted.org/pyDOE/.

Table 5
Levels of the factors for temporal and spatial SA.

Factor	Unit	Range II		
		−	+	Relative range(%)
κ^*		0.0088	0.0132	40
ν'		0.18	0.22	20
λ_i^*		0.0777	0.095	20
M_c		1.26	1.55	20
M_e		0.94	1.15	20
σ'_{p_0}	kPa	90	100	10
α_0		0.504	0.756	40
ω		24	36	40
ω_d		0.819	1.014	20
χ_0		8	12	40
a		6	9	40
b		0.36	0.54	40
μ_i^*		1.42×10^{-3}	2.13×10^{-3}	40
u (consolidation)		No	Yes	Qualitative

Table 6
$2_{\mathbf{IV}}^{14-9}$ design: table of contrast.

Run No.	κ^*	ν'	λ_i^*	M_c	M_e	ω	ω_d	a	b	σ'_{p_0}	α_0	χ_0	μ_i^*	u
1	−	−	−	−	−	−	−	−	−	−	−	−	−	−
2	+	−	−	−	−	+	+	+	+	+	+	+	−	−
3	−	+	−	−	−	+	+	+	+	−	−	−	+	+
4	+	+	−	−	−	−	−	−	−	+	+	+	+	+
5	−	−	+	−	−	+	+	−	−	+	+	−	+	+
6	+	−	+	−	−	−	−	+	+	−	−	+	+	+
7	−	+	+	−	−	−	−	+	+	+	+	−	−	−
8	+	+	+	−	−	+	+	−	−	−	−	+	−	−
9	−	−	−	+	−	+	−	+	−	+	−	+	+	−
10	+	−	−	+	−	−	+	−	+	−	+	−	+	−
11	−	+	−	+	−	−	+	−	+	+	−	+	−	+
12	+	+	−	+	−	+	−	+	−	−	+	−	−	+
13	−	−	+	+	−	−	+	+	−	−	+	+	−	+
14	+	−	+	+	−	+	−	−	+	+	−	−	−	+
15	−	+	+	+	−	+	−	−	+	−	+	+	+	−
16	+	+	+	+	−	−	+	+	−	+	−	−	+	−
17	−	−	−	−	+	+	−	−	+	−	+	+	−	+
18	+	−	−	−	+	−	+	+	−	+	−	−	−	+
19	−	+	−	−	+	−	+	+	−	−	+	+	+	−
20	+	+	−	−	+	+	−	−	+	+	−	−	+	−
21	−	−	+	−	+	−	+	−	+	+	−	+	+	−
22	+	−	+	−	+	+	−	+	−	−	+	−	+	−
23	−	+	+	−	+	+	−	+	−	+	−	+	−	+
24	+	+	+	−	+	−	+	−	+	−	+	−	−	+
25	−	−	−	+	+	−	−	+	+	+	+	−	+	+
26	+	−	−	+	+	+	+	−	−	−	−	+	+	+
27	−	+	−	+	+	+	+	−	−	+	+	−	−	−
28	+	+	−	+	+	−	−	+	+	−	−	+	−	−
29	−	−	+	+	+	+	+	+	+	−	−	−	−	−
30	+	−	+	+	+	−	−	−	−	+	+	+	−	−
31	−	+	+	+	+	−	−	−	−	−	−	−	+	+
32	+	+	+	+	+	+	+	+	+	+	+	+	+	+

The results are plotted in Fig. 7 in terms of the misfit function for a given parameter. The small embedded image plots demonstrate all the realisations. The results have been extracted at the same time, as shown in the embedded image, thus corresponding different effective stress levels. Fig. 7 shows that the most dominant factors of Zone I (the overconsolidation region) are κ^*, u, ν', and α_0. Also, notice that the small effects during the initial Zone are due to the lower variability in the model response. The changes in the elastic parameter κ^* have significant effects on the calibration of the initial flat portion of the consolidation curve. Because of the horizontal component of effective stress tensor, the elastic parameter ν' exhibits some effect. In addition anisotropy, α_0 has little effect on the

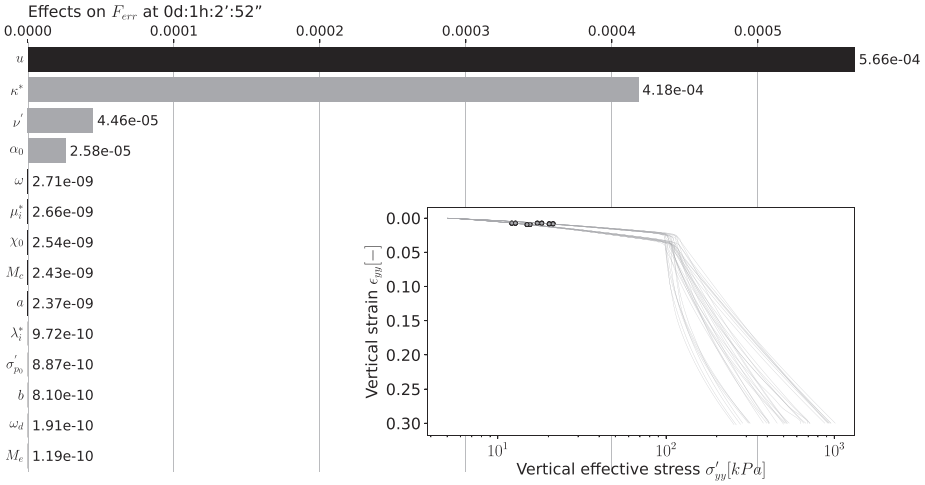

Fig. 7. Temporal effects of the $2^{14-9}_{\mathbf{IV}}$ fractional design corresponding to Zone I, *i.e.* taken at $1h:2':52''$ of the CRS realisations.

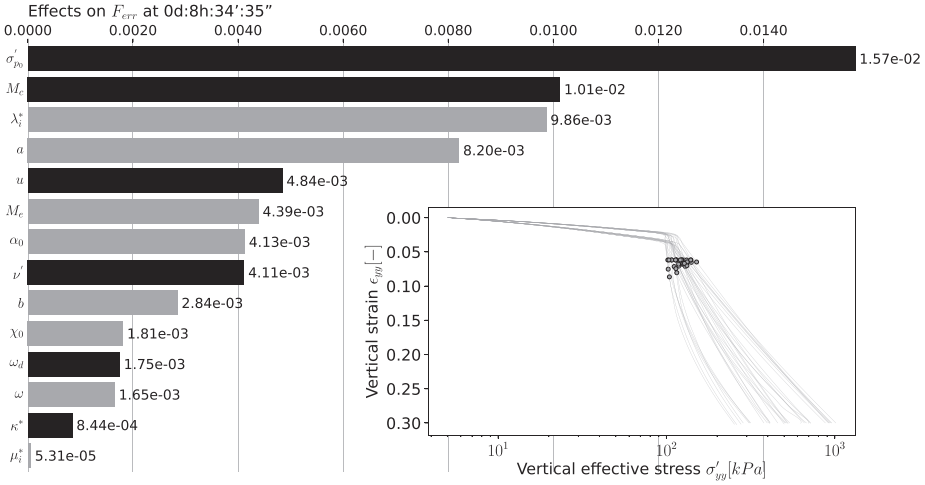

Fig. 8. Temporal effects of the $2^{14-9}_{\mathbf{IV}}$ fractional design corresponding to Zone II, *i.e.* taken at $8h:34':35''$ of the CRS realisations.

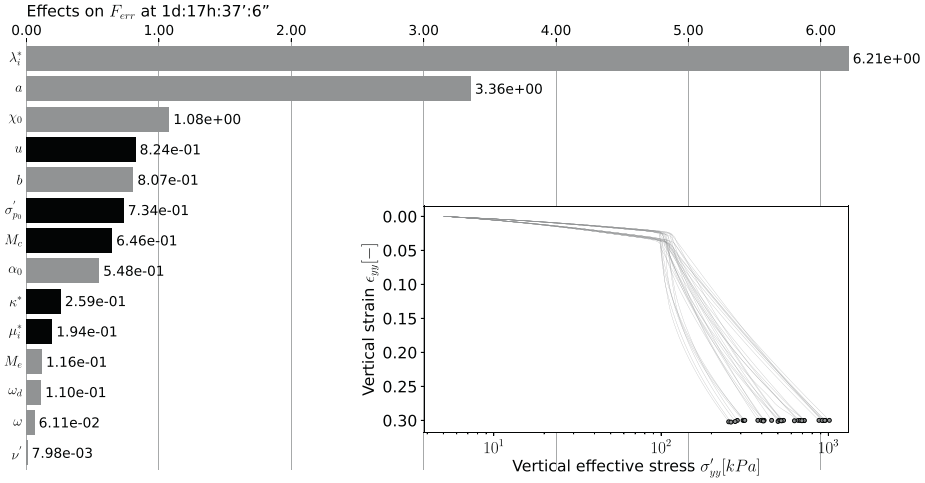

Fig. 9. Temporal effects of the $2^{14-9}_{\mathbf{IV}}$ design corresponding to Zone III, *i.e.* taken at : $1d:17h:37':6''$ of the CRS realisations.

initial response of the compression curve. This is due to the fact that the Creep-SCLAY1S model does not have a purely elastic region. Therefore, viscoplastic strains occur in all effective stress ranges, predicting negligible rotation of the yield curve. During the application of the constant displacement rate, the porewater will flow caused by the gradients of excess pore water pressure. Thus, the effect of consolidation u, *i.e.* the generation and dissipation of excess porewater pressures, during the initial stage of the test becomes evident over the discretised domain.

The most distinguishable factors of Zone II are $\sigma'_{p_0}, M_c, \lambda_i^*$, and a in Fig. 8. The preconsolidation pressure σ'_{p_0} defines the boundary between small and large irrecoverable strains by determining the initial size of the Normal Compression Surface (NCS). Thus, the initial input of σ'_{p_0} has major effect on the calibration of Zone II. Since large viscoplastic strains are predicted after yielding, the viscoplastic flow rule affects the ratio of volumetric and deviatoric strain increments. Therefore, the slope of the critical state line at compression M_c has significant effect on the transitional Zone II. The sensitivity of λ_i^* follows by transitioning to the second portion of the compression curve. The nature of bond degradation, *i.e.* also referred to as destructuration, indicates slippage and rearrangements of soil particles that changes the nature of the inter-particle forces leading to bond degradation (Karstunen et al., 2005). Thus, as in Zone II an increasing amount of viscoplastic strains are being predicted, the importance of the destructuration parameter a has grown.

In Fig. 9, the main effects of factors λ_i^*, a, and χ_0 stand out. The most striking effect on the misfit function results from the intrinsic modified compression index (λ_i^*) given that is the ultimate target value for the inclination of the effective stress–strain curve once all bonds have been destroyed by the viscoplastic work. Consequently, a change in the value of this parameter has significant effects on the calibration of the CRS loading path during the post failure zone. Since there are substantial viscoplastic strains, the importance of destructuration parameter a is noticeable. Furthermore, the influence of an appropriate initial state variable, such as χ_0 that governs the initial bonding is highlighted over the post yield region.

In general, the temporal assessment illustrates that the hierarchical features of the constitutive model are in-line with the physics of the consolidation problem. Figs. 7–9 demonstrate the transient nature of the significance of particular model parameters at different phases of consolidation. This reveals the non-stationary nature of factor screening for time-dependent processes, such as the CRS loading path, as clearly the ranking of the significant parameters evolves over time. Following the temporal SA, the parameters with detectable influence are identified as *active* parameters for each Zone defined; see Eq. (7). The underlined parameters in Eq. (7) are denoted as the most dominant for the calibration of the CRS boundary value problem using Creep-SCLAY1S. Fig. 10(a) illustrates the problem of non-uniqueness due to variation of the ω while keeping the other parameters constant. As a result, similar

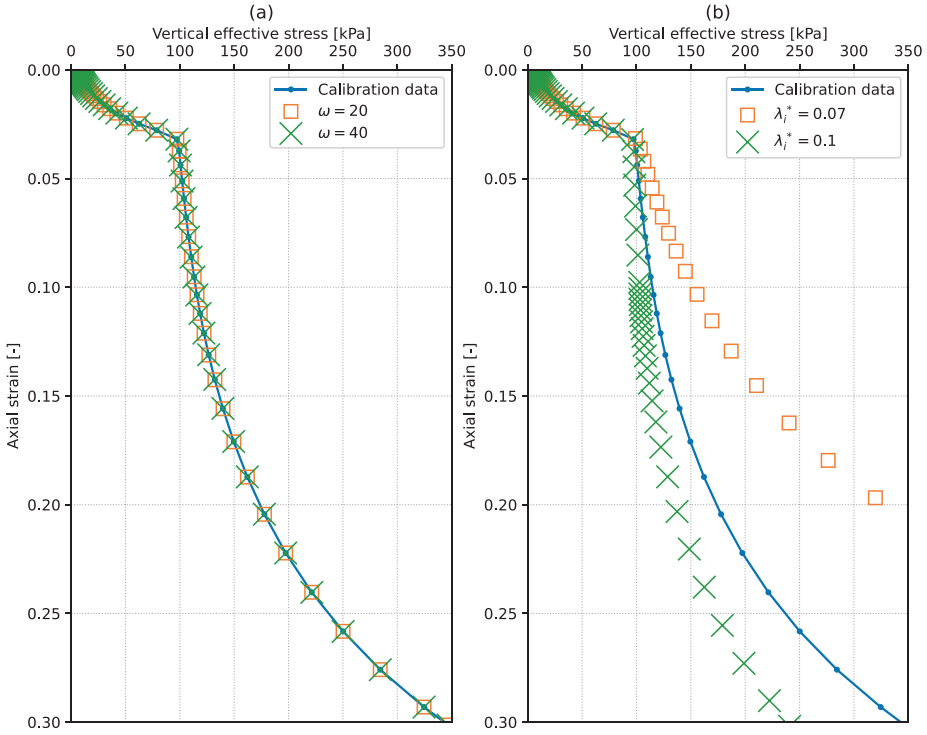

Fig. 10. Demonstration of non-uniqueness for parameter sets in CRS loading path using Creep-SCLAY1S. (a) Parameter ω results in non-uniqueness. (b) Changing λ_i^* yields unique curves after the preconsolidation pressure.

solutions have been obtained for stress–strain behaviour by changing the non-influential parameter of ω. However, Fig. 10(b) shows that the governing parameters from temporal SA, such as λ_i^*, leads to unique solutions within their influential Zones. The method introduced in this paper systematically indicated active parameters that lead to unique solutions. In essence, this information is beneficial for calibration procedures by fixing the inactive parameters chronologically; hence, the problem of non-uniqueness is likely to be limited as well as the necessary number of trials. Although different parameter sets for end Zones were introduced, the uniqueness of input parameters is fulfilled over the entire stress–strain curve, pinpointing the advantage of DOE while examining the possible combinations of levels studied. It is therefore noteworthy that, despite intersective parameters in different Zones, the uniqueness of input parameters must be provided for further calibration purposes.

$$\text{zone I} = \{\underline{\kappa^*}, \underline{u}, \nu', \alpha_0\} \tag{7a}$$

$$\text{zone II} = \left\{\underline{\sigma'_{p_0}}, \underline{M_c}, \underline{\lambda_i^*}, \underline{a}, \kappa^*, u\right\} \tag{7b}$$

$$\text{zone III} = \left\{\underline{\lambda_i^*}, \underline{a}, \underline{\chi_0}, u, b, \sigma'_{p_0}, M_c, \alpha_0\right\} \tag{7c}$$

5.2. Spatial SA of the boundary value problem

In addition to the temporal response emerging from consolidation, FE modelling enables investigating the effect of each factor as a function of its spatial coordinate. The parameter set corresponding to the final stage of the CRS loading path, *i.e.* Zone III, is examined further using spatial SA.

As a coupled formulation was used in all FE simulations, the factor u has been excluded in the next stage of investigation. Instead, the effect of the displacement rate in the CRS simulations have been investigated in order to examine the rate-dependent response of the numerical model. The plausible rate of displacements is altered from 0.0006 to 0.02 mm min^{-1} following the experiments reported in Sallfors (1975). The bounds of the Creep-SCLAY1S parameters obtained from Eq. (7c) remain the same as Table 5; consequently, eight factors are selected to construct the Experimental Design. The main aim is to examine the spatial sensitivity patterns using a two-level full factorial design and Sobol method. The two-level full factorial design yields 256 realisations, whereas the Sobol method requires 18 000 simulations. The sensitivity measures over the spatial domain are normalised between 0 and 1, in which 1 denotes the highest level of importance. Fig. 11 displays the spatial sensitivity maps of the three most significant model parameters at the end of the CRS stress path. The observation has been made by comparing Sobol's first-order index S_i to the main effects of the full factorial study. The sensitivity maps using the two GSA methods are comparable to a large extent, as depicted in Fig. 11. For instance, the effect of displacement rate are most pronounced near the top boundary for both methods. By noticing that the spatial SA is performed at the end of the loading path, destructuration parameters a and χ_0 are shown to be sensitive towards the middle and bottom of the specimen, respectively. The obtained patterns exhibit 1D gradual changes of sensitivity, *i.e.* in line with the behaviour of the CRS test under oedometric compression.

Concerning the two GSA methods, some differences are noticed in the a and χ_0 maps, which may result from the different sampling schemes of the two methods. Overall, the spatially distributive sensitivity maps in Fig. 11 have revealed the locations where the parameters have greatest importance. Given the spatial patterns of two GSA methods are analogous, the Experimental Design is also able to provide accurate sensitivity maps. Fig. 12 presents the most notable interactive effect, *i.e.* captured between parameters λ_i^* and a. Thus, the impacts of these two model parameters must be considered simultaneously over the course of large viscoplastic strains. The representations

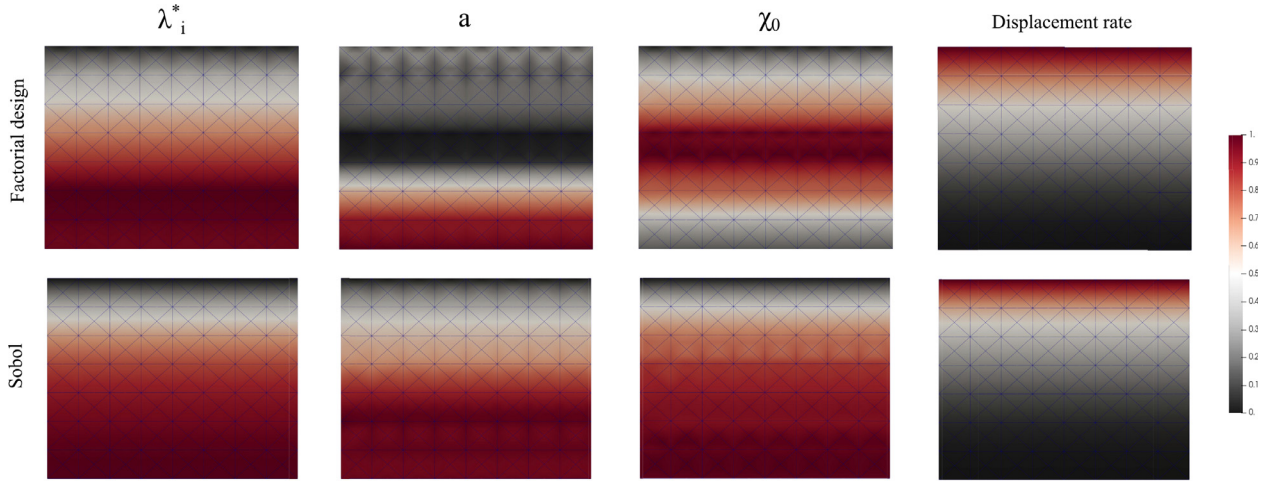

Fig. 11. Sensitivity maps towards the vertical effective stress on spatial domain.

indicate that the interaction takes place since an increase in λ_i^* reduces the predicted vertical effective stress at both levels of a. However, at a higher level of a the specimen resists lower stress levels than of a lower level of a.

At laboratory scale, the spatial assessment provides an essential step towards calibration of advanced models against experimental mesoscale data. Such experimental data includes three-dimensional fields of strain that is collected from the sample by using X-ray Computed Tomography (XCT) techniques (*e.g.* Birmpilis et al., 2022). The spatial assessment is essential for field scale modelling, where stress fields are non–homogeneous as different parts of the system experiencing different loading paths at different magnitudes. In addition, the spatial location of factors differs for boundary value problems in Geotechnics, as illustrated in the temporal assessment.

5.3. Execution time and storage costs

Experimental Design is an economical GSA method in order to assess boundary value problems. We present data on running time and the amount of storage space required for each assessment step. Table 7 summarises information regarding assessment steps used in this study. The convergence study that the Sobol method requires, come with many trials, which yields higher computational costs, whereas the combination of fractional and full factorial design requires less storage and execution time. This is crucial for deterministic Geotechnical FE models, in which a single realisation may take a substantial amount of time. Fig. 13 shows that, on average, the analyses performed using the Sobol method have taken up almost 77 times as much storage as Experimental Design. By comparing the two GSA methods performed for spatial SA, computational time has been increased almost 300 times by using the Sobol method. Considering the high computational burden of the Sobol method, especially for sensitivity analysis purposes, the appropriate Design of Experiments resulted in tremendous savings without inaccuracy in the solution.

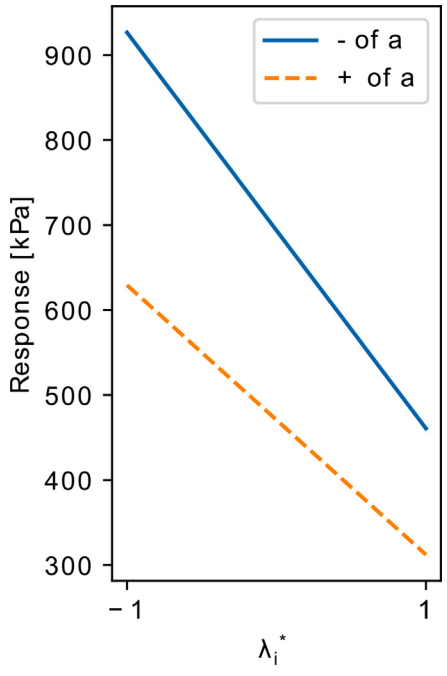

Fig. 12. Changes in the predicted vertical effective stress by modified intrinsic index λ_i^* for two levels of destructuration parameter a.

6. Conclusions

The response of a rate-dependent numerical model, considering a Constant Rate of Strain (CRS) test using Finite Element (FE) analysis, were assessed by means of Experimental Design. The FE model of the CRS tests included complexities, such as advanced rate-dependent constitutive model for natural soft clays and a coupled formulation for consolidation. The results demonstrate that Experimental Design was successfully implemented and benchmarked against the Sobol method using FE modelling. The study draws several conclusions regarding the optimal calibration of CRS loading path, as well as the implementation of Experimental Design in FE modelling.

Regarding the optimal calibration of the numerical model, it was shown that the relative significance of the model parameters vary in different zones of the effective stress–strain curve resulting from CRS testing; see Eqs. (7a), (7b), (7c). This was accomplished by defining a temporal misfit function with respect to a calibrated model, in which a fractional factorial design of Resolution IV determined the important parameters. The results of this approach identified the parameters of the constitutive model that lead to non-unique solutions for the CRS loading path at system-level. The findings of temporal SA also illustrated the evolving significance of Creep-SCLAY1S model parameters, highlighting the non-stationary essence of parameter screening for such problems.

In addition, the sensitivity of model parameters from Eq. (7c) were studied in spatial domain, pinpointing the precise spacial location of sensitive factors. For this purpose, the result of full factorial Experimental Design was compared to the Sobol method. The obtained sensitivity maps were in good agreement. The results of spatially distributive sensitivity maps potentially offer opportunities to detect and screen important parameters for subsequent statistical analyses that incorporate spatial heterogeneity, such as the Random Finite Element Method (RFEM) or sensor installation as part of inverse modelling strategies for data monitoring. It was also highlighted that quantification of interactive effect was a beneficial feature of Experimental Design. A noticeable interaction effect between the modified compression index λ_i^* and absolute rate of destructuration a has been detected. The interaction effect between λ_i^* and a occurred post-yield where large viscoplastic strains were generated, meaning that both factors must not be

Table 7
The required total number of realisations.

Assessment steps	Scaling	k	N	Total realisations
Sobol convergence study	$(2k+2)N$	13	$[500 \sim 1000]$	126 000
Temporal SA: fractional design	2^{k-9}_{IV}	14	×	32
Spatial SA: Sobol	$(2k+2)N$	8	1000	18 000
Spatial SA: full factorial	2^k	8	×	256

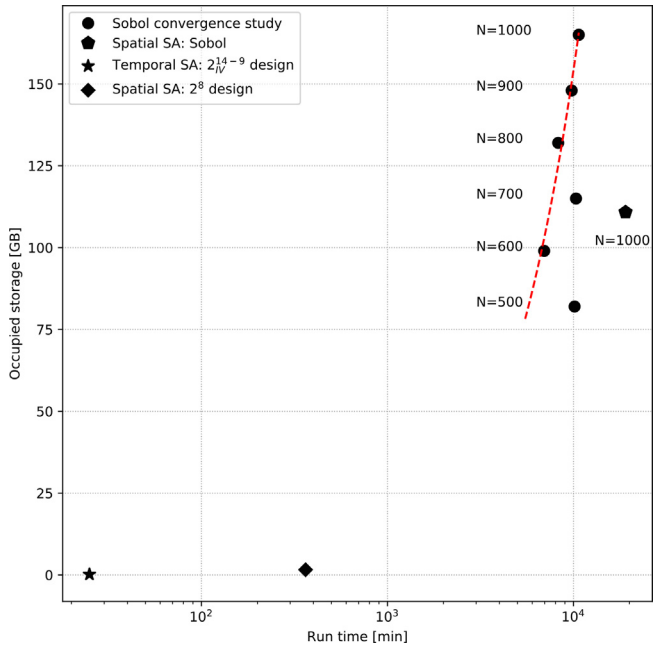

Fig. 13. Execution time and required storage.

interpreted independently, as they are part of the same hardening law in Creep-SCLAY1S.

It may be concluded that Experimental Design proved to be a promising approach to assess rate-dependent numerical models. The Sobol method consumed more computational time as well as required storage capacity. By using Experimental Design for spatial SA, the savings in terms of computational time was as high as 18 500 min. Moreover, 109 GB storage was saved. Therefore, an appropriately executed Design of Experiments reduces the efforts towards the assessment and calibration of Geotechnical FE numerical models without sacrificing accuracy.

Acknowledgements

The financial support from the Swedish Transport Administration in the framework of BIG (Branch samverkan i Grund) under Grant No. TRV 2019/30856 is greatly acknowledged. JD is supported by FORMAS under Grant No. 2016–01070. The work is performed as part of Digital Twin Cities Centre that is supported by Sweden's Innovation Agency VINNOVA. Finally, Prof. Minna Karstunen's valuable comments on this paper are greatly appreciated.

Appendix A. Brief overview of Creep-SCLAY1S

For full details of Creep-SCLAY1S in its generalised state, the reader is referred to Gras et al. (2018) and Sivasithamparam et al. (2015). The stress-state of the Creep-SCLAY1S model in triaxial space includes three main surfaces *i.e.* inclined by the anisotropy scalar α; see Fig. 14. The shape and orientation of all surfaces are similar and defined according to Eq. (A.8):

$$f_{\text{surface}} = (q - \alpha p')^2 - \left(M(\theta)^2 - \alpha^2\right)\left(p'_{\text{surface}} - p'\right)p' = 0 \tag{A.8}$$

In Eq. (A.8), M controls the stress ratio at a critical state and is a function of the modified Lode angle θ,

- Normal Consolidation Surface (NCS): A boundary surface between the small and large viscoplastic strains. Note that elastic and viscoplastic strains are generated for all stress states, only the magnitude of the viscoplastic strain rate substantially increases when the current stress is beyond the NCS. The size of this surface is determined by the preconsolidation pressure projected on the isotropic axis p'_m.

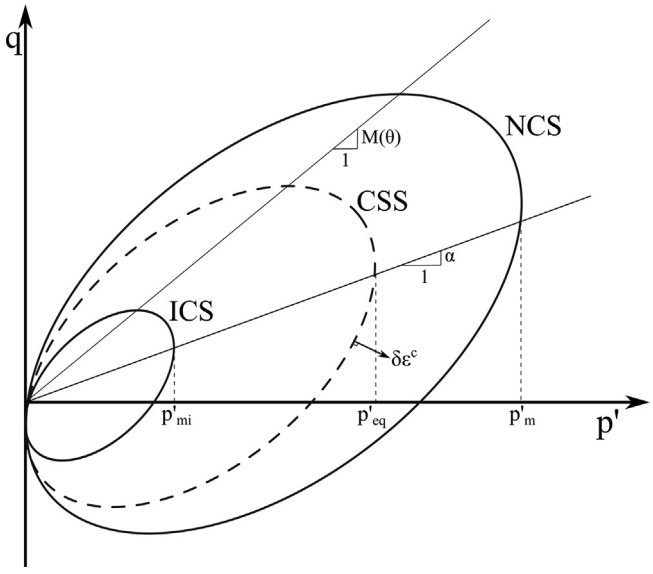

Fig. 14. Creep-SCLAY1S and its associated surfaces (Gras et al., 2018).

- Current Stress Surface (CSS): A surface that tracks the current state of effective stress and its size is controlled by the mean effective stress p'_{eq}.
- Intrinsic Compression Surface (ICS): This state represents an imaginary soil sample without bonding, but supplied with a similar void ratio and fabric of the NCS surface. The size of ICS is determined by the intrinsic isotropic preconsolidation pressure p'_{mi}, in which the size of ICS and NCS is linked together by a bonding parameter χ given in Eq. (A.9).

$$p'_m = (1+\chi)p'_{mi} \tag{A.9}$$

The total strain rate is given by the summation of the elastic and viscoplastic (creep) strain rates in volumetric and deviatoric decomposition:

$$\begin{aligned}\dot{\epsilon}_v &= \dot{\epsilon}^e_v + \dot{\epsilon}^c_v \\ \dot{\epsilon}_d &= \dot{\epsilon}^e_d + \dot{\epsilon}^c_d\end{aligned} \tag{A.10}$$

The viscoplastic strain rates in Eq. (A.10) are defined using the associated flow rule:

$$\begin{aligned}\dot{\epsilon}^c_v &= \dot{\Lambda}\frac{\partial p'_{eq}}{\partial p'} \\ \dot{\epsilon}^c_d &= \dot{\Lambda}\frac{\partial p'_{eq}}{\partial q}\end{aligned} \tag{A.11}$$

In which $\dot{\Lambda}$ is the rate-dependent viscoplastic multiplier:

$$\dot{\Lambda} = \frac{\mu^*_i}{\tau}\left(\frac{p'_{eq}}{p'_m}\right)^{\frac{\lambda^*_i-\kappa^*}{\mu^*_i}}\left(\frac{M(\theta)^2-\alpha^2_{K^{nc}_0}}{M(\theta)^2-\eta^2_{K^{nc}_0}}\right) \tag{A.12}$$

The model consists of three hardening laws:

- Volumetric hardening law: The rate of the viscoplastic volumetric strain governs the size of the ICS; see Eq. (A.13).

$$\dot{p}'_{mi} = \frac{p'_{mi}}{\lambda^*_i-\kappa^*}\cdot\dot{\epsilon}^c_v \tag{A.13}$$

- Rotational hardening law: The rotational hardening law captures the evolving anisotropy by incorporating the rate of the volumetric viscoplastic strain $\dot{\epsilon}^c_v$ and the deviatoric viscoplastic strain $\dot{\epsilon}^c_d$ (Wheeler et al., 2003); see Eq. (A.14).

$$\dot{\alpha} = \omega\left[\left(\frac{3q}{4p'}-\alpha\right)\left\langle\dot{\epsilon}^c_v\right\rangle + \omega_d\left(\frac{q}{3p'}-\alpha\right)\left|\dot{\epsilon}^c_d\right|\right] \tag{A.14}$$

- Destructuration hardening law: Eq. (A.15) incorporates the degradation of the fabric structure by introducing two new parameters, *i.e.* the absolute and relative rate of destructuration (a & b). In this assumption, both the volumetric and deviatoric viscoplastic strain tend to decrease the bonding parameter χ until it totally vanishes to zero, *i.e.* an irreversible degradation of the initial bonding (Karstunen et al., 2005).

$$\dot{\chi} = -a\chi\left(\left|\dot{\epsilon}^c_v\right| + b\left|\dot{\epsilon}^c_d\right|\right) \tag{A.15}$$

In general, Creep-SCLAY1S requires 14 input parameters that are summarised in Table 4.

References

Amavasai, A., Sivasithamparam, N., Dijkstra, J., Karstunen, M., 2018. Consistent Class A & C predictions of the Ballina test embankment. Comput. Geotech. 93, 75–86.

Birmpilis, G., Ando, E., Stamati, O., Hall, S.A., Gerolymatou, E., Dijkstra, J., 2022. Experimental quantification of 3D deformations in sensitive clay during stress-probing. Geotechnique, 1–12.

Box, G.E.P., Draper, N.R., 1987. Empirical Model-Building and Response Surfaces. Wiley Series in Probability and Statistics. Wiley.

Box, G.E.P., Hunter, J.S., Hunter, W.G., 2009. Statistics for Experimenters; Design, Innovation, and Discovery. John Wiley & Sons Inc, Hoboken, New Jersey, pp. 1–655.

Crisp, M., Jaksa, M., Kuo, Y., Fenton, G., Griffiths, D., 2021. Characterizing site investigation performance in a two layer soil profile. Can. J. Civ. Eng. 48 (2), 115–123.

Czitrom, V., 1999. One-factor-at-a-time versus designed experiments. Am. Statist. 53 (2), 126–131.

Dafalias, Y.F., Manzari, M.T., Papadimitriou, A.G., 2006. SANICLAY: simple anisotropic clay plasticity model. Int. J. Numer. Anal. Meth. Geomech. 30 (12), 1231–1257.

Fang, Y., Su, Y., 2020. On the use of the global sensitivity analysis in the reliability-based design: Insights from a tunnel support case. Comput. Geotech. 117.

Fenton, G.A., Griffiths, D.V., 1993. Statistics of Block Conductivity Through a Simple Bounded Stochastic Medium. Water Resour. Res. 29 (6), 1825–1830.

Fenton, G.A., Vanmarcke, E.H., 1990. Simulation of Random Fields via Local Average Subdivision. J. Eng. Mech. 116 (8), 1733–1749.

Ferretti, F., Saltelli, A., Tarantola, S., 2016. Trends in sensitivity analysis practice in the last decade. Sci. Total Environ. 568, 666–670.

Gras, J.-P., Sivasithamparam, N., Karstunen, M., Dijkstra, J., 2017. Strategy for consistent model parameter calibration for soft soils using multi-objective optimisation. Comput. Geotech. 90, 164–175.

Gras, J.-P., Sivasithamparam, N., Karstunen, M., Dijkstra, J., 2018. Permissible range of model parameters for natural fine-grained materials. Acta Geotech. 13 (2), 387–398.

Griffiths, D.V., Fenton, G.A., 1993. Seepage beneath water retaining structures founded on spatially random soil. Geotechnique 43 (4), 577–587.

Herman, J., Usher, W., 2017. SALib: An open-source Python library for Sensitivity Analysis. J. Open Source Softw. 2 (9).

Homma, T., Saltelli, A., 1996. Importance measures in global sensitivity analysis of model output. Reliab. Eng. Syst. Saf. 52, 1–17.

Journel, A.G., Alabert, F., 1989. Non-Gaussian data expansion in the Earth Sciences. Terra Nova 1 (2), 123–134.

Karlsson, M., Emdal, A., Dijkstra, J., 2016. Consequences of sample disturbance when predicting long-term settlements in soft clay. Can. Geotech. J. 53 (12), 1965–1977.

Karstunen, M., Amavasai, A., 2017. BEST SOIL: Soft soil modelling and parameter determination. Tech. Rep. Gothenburg, Sweden: Department of Architecture and Civil Engineering, Chalmers University of Technology, pp. 78.

Karstunen, M., Krenn, H., Wheeler, S.J., Koskinen, M., Zentar, R., 2005. Effect of Anisotropy and Destructuration on the Behavior of Murro Test Embankment. Int. J. Geomech. 5 (2), 87–97.

Kashef, A.I., 1986. Groundwater Engineering. McGraw-Hill Book Company, pp. 1–512.

Khaledi, K., Mahmoudi, E., Datcheva, M., Konig, D., Schanz, T., 2016. Sensitivity analysis and parameter identification of a time dependent constitutive model for rock salt. J. Comput. Appl. Math. 293, 128–138.
Leroueil, S., Vaughan, P.R., 1990. The general and congruent effects of structure in natural soils and weak rocks. Geotechnique 40 (3), 467–488.
Liu, W., Wu, X., Zhang, L., Zheng, J., Teng, J., 2017. Global Sensitivity Analysis of Tunnel-Induced Building Movements by a Precise Metamodel. J. Comput. Civil Eng. 31 (5).
Mahmoudi, E., Holter, R., Georgieva, R., Konig, M., Schanz, T., 2019. On the Global Sensitivity Analysis Methods in Geotechnical Engineering: A Comparative Study on a Rock Salt Energy Storage. Int. J. Civil Eng. 17 (1), 131–143.
Masin, D., 2005. A hypoplastic constitutive model for clays. Int. J. Numer. Anal. Meth. Geomech. 29 (4), 311–336.
Miro, S., Hartmann, D., Schanz, T., 2014. Global sensitivity analysis for subsoil parameter estimation in mechanized tunneling. Comput. Geotech. 56, 80–88.
Mitchell, J., Soga, K., 2005. Fundamentals of Soil Behavior, 3rd ed. Wiley.
Montgomery, D.C., 2009. Design and analysis of experiments, 7th ed. John Wiley and sons, Hoboken, New Jersey, p. 656.
Muir Wood, D., 2004. Geotechnical Modelling. Taylor & Francis.
Muir Wood, D., 2016. Analysis of consolidation with constant rate of displacement. Can. Geotech. J. 53 (5), 740–752.
Nishimura, S.-I., Nishiyama, T., Murakami, A., 2005. Inverse analysis of soft grounds considering nonlinearity and anisotropy. Soils Found. 45 (2), 87–95.
Nishimura, S.-I., Shimada, K., Fujii, H., 2002. Consolidation inverse analysis considering spatial variability and non-linearity of soil parameters. Soils Found. 42 (3), 45–61.
Ottosen, N.S., Petersson, H., 1992. Introduction to the Finite Element Method. Prentice-Hall.
Papon, A., Riou, Y., Dano, C., Hicher, P.-Y., 2012. Single-and multi-objective genetic algorithm optimization for identifying soil parameters. Int. J. Numer. Anal. Meth. Geomech. 36 (5), 597–618.
Peck, R.B., Hanson, W.E., Thornburn, T.H., 1974. Foundation Engineering. John Wiley & Sons, Inc., Hoboken, New Jersey.
Phoon, K.-K., Kulhawy, F.H., 1999. Characterization of geotechnical variability. Can. Geotech. J. 36 (4), 612–624.
Potts, D.M., Zdravkovic, L., 2001. Finite Element Analysis in Geotechnical Engineering. Thomas Telford.
Roscoe, K., Burland, J., 1968. On the generalised stress-strain behaviour of wet clay. Eng. Plast., 535–609
Rowe, R.K., Hinchberger, S.D., 1998. The significance of rate effects in modelling the Sackville test embankment. Can. Geotech. J. 35 (3), 500–516.
Sallfors, G., 1975. Preconsolidation pressure of soft, high-plastic clays. PhD thesis. Chalmers University of Technology.
Saltelli, A., 2002. Making best use of model evaluations to compute sensitivity indices. Comput. Phys. Commun. 145 (2), 280–297.
Saltelli, A., Annoni, P., 2010. How to avoid a perfunctory sensitivity analysis. Environ. Modell. Softw. 25 (12), 1508–1517.
Saltelli, A., Ratto, M., Andres, T., Campolongo, F., Cariboni, J., Gatelli, D., Saisana, M., Tarantola, S., 2008. Global Sensitivity Analysis: The Primer. John Wiley & Sons, Ltd, Chichester, UK, p. 312.
Shao, D., Jiang, G., Zong, C., Xing, Y., Zheng, Z., Lv, S., 2021. Global sensitivity analysis of behavior of energy pile under thermo-mechanical loads. Soils Found. 61 (2), 283–302.
Sivasithamparam, N., Karstunen, M., Bonnier, P., 2015. Modelling creep behaviour of anisotropic soft soils. Comput. Geotech. 69, 46–57.
Sobol', I.M., 1993. Sensitivity Estimates for Nonlinear Mathematical Models. MMCE (English translation from Russian paper) 1, 407–414.
Tarantola, A., 2005. Inverse Problem Theory and Methods for Model Parameter Estimation. SIAM.
Tochnog Professional, n.d.. Tochnog Professional, Free Finite Element Software.
Tornborg, J., Karlsson, M., Kullingsjo, A., Karstunen, M., 2021. Modelling the construction and long-term response of Gota Tunnel. Comput. Geotech. 134, 104027.
Verruijt, A., 2015. Theory and Problems of Poroelasticity. Delft University of Technology.
Wheeler, S., Naatanen, A., Karstunen, M., Lojander, M., 2003. An anisotropic elastoplastic model for soft clays. Can. Geotech. J. 40 (2), 403–418.
Yin, Z.-Y., Chang, C.S., Karstunen, M., Hicher, P.-Y., 2010. An anisotropic elastic-viscoplastic model for soft clays. Int. J. Solids Struct. 47 (5), 665–677.
Yin, Z.-Y., Jin, Y.-F., Shen, J.S., Hicher, P.-Y., 2018. Optimization techniques for identifying soil parameters in geotechnical engineering: comparative study and enhancement. Int. J. Numer. Anal. Meth. Geomech. 42 (1), 70–94.
Zhao, C., Lavasan, A.A., Holter, R., Schanz, T., 2018. Mechanized tunneling induced building settlements and design of optimal monitoring strategies based on sensitivity field. Comput. Geotech. 97, 246–260.